An apparatus for imaging liquids, cells, and other wet samples in the scanning electron microscopy

S. Thiberge
Department of Physics Complex Systems, The Weizmann Institute of Science, 76100 Rehovot, Israel

O. Zik
Quantomix Ltd., 12 Hamada Street, Park Tamar, 76000 Rehovot, Israel and El-Mul Technologies, Yavne, Israel

E. Moses[a)]
Department of Physics Complex Systems, The Weizmann Institute of Science, 76100 Rehovot, Israel

(Received 30 January 2003; accepted 5 April 2004; published online 21 June 2004)

We present a technique of scanning electron microscopy that is adapted to the study of wet samples. The wet environment is protected in a small chamber enclosed by a membrane, which is thin enough for energetic electrons to go through and interact with the sample studied. We detail both the technique and the general mechanisms of signal formation in the imaging of samples through a membrane. We first describe our setup and the properties required for the membrane, the main element in this method. Some simple measurements for its characterization are given, guiding the choice of material and thickness. We then go on to describe the capabilities of the technique in imaging a variety of different samples. We evaluate the accessible contrast and resolution, and the current needed to obtain them. Low contrast samples can be imaged with an improvement in resolution over optical microscopy. High contrast samples like gold markers labeling a biological cell can be imaged with a resolution of the order of 10 nm. The resolution depends on the location of the particle in the sample: the closer to the membrane, the better the resolution. We believe such a result opens up potential applications for routine experiments in biology, and expect this new technique to find numerous applications in domains where liquid samples are investigated such as soft materials science. © *2004 American Institute of Physics.* [DOI: 10.1063/1.1763262]

I. INTRODUCTION

Scanning microscopy techniques have seen an enormous advance in recent decades,[1–6] driven by the ever increasing demand for the imaging of smaller and smaller scales, far below the resolution of light. In this article we present the development of a new capability for the imaging of wet samples in the scanning electron microscope (SEM), a need that arises in the material, medical, and biological sciences. Such measurements have until now been limited by the need of sustaining the samples in a relative vacuum. Our system is based on the isolation of the fluid sample from the vacuum by the introduction of a membranous partition. Recent developments in polymer technology enable the production of thin membranes that are practically transparent to energetic electrons, yet are tough enough to withstand atmospheric pressures on one side and high vacuum on the other side. The imaged volume is the close proximity of the membrane, typically a few microns into the fluid. This is ideal for the inspection of objects that are stuck to the surface such as adherent biological cells. Our technique is furthermore easily adaptable to all existing scanning electron microscopes, enabling measurements of wet samples at room temperature and at atmospheric pressure.

The approach we use was proposed and already tried at the advent of the SEM,[7] but was subsequently rejected, mostly because of the unavailability of adequate materials. The material of choice at the time was colloidion, which was both unwieldy and resulted in unacceptably low resolution. The technique was left behind while users turned to the promise of alternative approaches, such as fixation of cells followed by gold evaporation. The idea of using a thin film as a separator between sample and vacuum can be found in some of the early approaches to environmental chambers, and has met with some success in the context of the transmission electron microscope,[8–13] but was never applied to the SEM. The physics behind the image forming mechanism in these two modes of electron microscopy are in any case very different.

We have shown that images of cells in a wet environment can be obtained with this technique.[14] Cell structures that can also be immuno-gold labeled or stained are easily imaged. The method can be applied to a variety of different kinds of wet samples, not only cells but other tissue samples and complex fluids such as polymeric or micellar solutions as well.

The membrane is the central part of this method. Beyond several mechanical properties such as sturdiness and flexibility, one of the most important requirements of a membrane is that the electron beam interacts as little as possible with it. In this publication we characterize in detail the interaction of

a)Author to whom correspondence should be addressed; electronic mail: elisha.moses@weizmann.ac.il

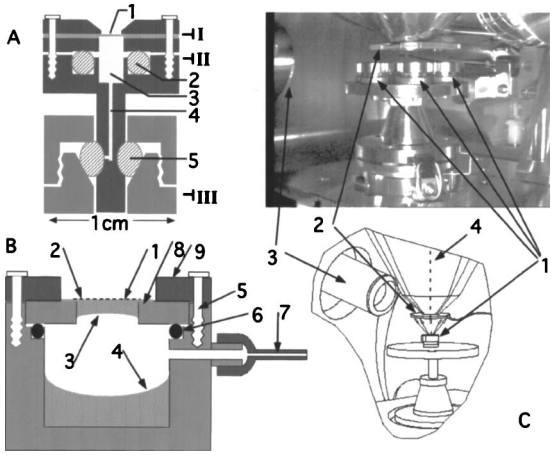

FIG. 1. (A) Chamber I: atmospheric pressure chamber setup. The membrane (1) is mounted on a plastic ring of inner diameter 2.8 mm. A TEM Ni grid is attached to the external side of the membrane to minimize the risk of rupture because of the difference of pressure between the vacuum outside and the fluid inside. The whole membrane assembly is sandwiched between two stainless steel pieces, thus forming part I. The second part II is built on the basis of a conventional specimen mount for the SEM (diameter 12.7 mm, pin diameter 3.2 mm). A small cavity (3) is drilled in the middle and a thin channel (4) joins the cavity to a small hole located at the middle height of the mounting pin. When preparing the sample, parts I and II are first fully filled with fluid. Then they are assembled together using o-ring (2) while excess fluid is drained from the chamber through the bottom aperture. A second o-ring (5) is then put onto the pin to seal the bottom aperture. Part III screws on to seal the chamber assembly completely, pressing the second o-ring against the aperture. Although the sketch is not exactly to scale, the arrow sets the (noncritical) dimensions for both Chambers I and II. (B) Chamber II: low pressure chamber setup. The membrane (1) and the grid (2) are mounted on a perspex ring (8) with inner diameter 6 mm and thickness 3 mm. The cavity thus formed is filled with the liquid sample (3) of about 90 μl. The bottom of the chamber (12 mm inner diameter) is filled with a reservoir (4) of pure water (100–200 μl). The ring is assembled to the chamber using an o-ring (6). The assembly is pressed by an aluminum part (9) positioned on the top and attached by screws (5). The release apertures (7) have a 100 μm inner diameter and are 10–50 mm long. (C) Positioning of chambers (either I or II) inside an ESEM. Top is an image showing a multiple chamber setup and the bottom is a schematic of the ESEM. At the top three chambers are visible (1), while only one is shown at bottom. Multiple chambers can be rotated into place and viewed one by one. The relative positioning of the BSE (2) and SE (3) detectors is depicted. The path of the electron beam (4) is pointed out for clarity in the sketch.

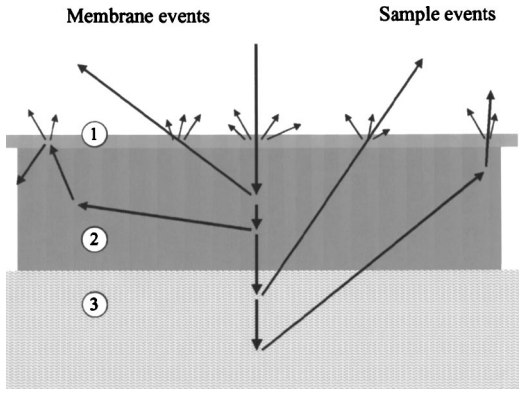

FIG. 2. Schematic of events giving rise to the *membrane* and the *sample* components of the signal. The upper dark gray region (1) represents an optional carbon-coated shield. The middle gray region (2) is the membrane itself, while the lower hatched region (3) is the sample. The middle thick arrows represent the incoming beam of electrons. SE escaping the sample are represented by short thin arrows, while BSE are represented by thin long arrows. When the beam penetrates the membrane, SE is emitted. These are ''membrane events'' such as the two events shown on the left. The two events on the right both carry ''sample'' information through the backscattered electrons and/or the secondary electrons generated by backscattered electrons approaching the top surface.

the beam with the membrane, giving some insight for the choice of a membrane for the purpose of wet SEM. We review in detail the signal formation mechanism and give a method to measure the beam–membrane interaction and to characterize the membrane. We also make a full evaluation of the minimum contrast observable with the membrane we use, and observe the resolution which can be obtained in different situations. We show that this method can even be used to measure the backscattering coefficients of liquid.

II. MICROSCOPE INSERTS

Sketches of two variations of the setup are shown in Fig. 1, to be used independently for different applications. Chamber I addresses the various liquid samples and maintains them at atmospheric pressure. Chamber II is specifically designed to maintain samples with water at low pressure. All parts of the sample chambers are numbered in the figures and described in the captions. For Chamber I, sealing of the sample against the external pressure difference is done with a series of o-rings. Closing the sample presents a hazard to the membrane, since considerable deformation would be caused if we were to compress the fluid inside. To avoid this, a small release channel is kept open through the stem of the insert, equilibrating the pressure inside by a slight release of fluid. The opening to the channel is subsequently sealed off with another o-ring that is screwed in place.

Decreasing the forces applied on the membrane is the motivation for the design of Chamber II. This design reduces the risk of rupture, and in this way very thin membranes can be used. The idea is to keep an open channel between the sample and the microscope chamber. When the microscope is evacuated, the pressure at the sample is close to the water vapor pressure. The aperture is chosen so that the evaporation occurs at a very slow rate, and we measured about 50 μl/h. The sample volume is usually between 80 and 100 μl. To diminish the evaporation from the sample itself, the chamber can contain a reservoir of pure water. In practice, working for several hours with the same sample presents no difficulty.

We used a JEOL 6400 SEM and a Philips XL30 ESEM-FEG microscope. Chamber I can obviously be used with any SEM, while Chamber II was used in the ESEM microscope. Because of the vapor release, it seems more natural to work in the mode called ''low vacuum,'' one of three functioning modes of this microscope. In this mode a small amount of water vapor is present in the microscope chamber, and we usually worked at a pressure equal or below 0.1 Torr. However, the amount of vapor exiting our chamber is easily handled by the microscope's pump, and we discovered that we can work just as well in the ''high-vacuum'' mode. This has no particular advantage with the ESEM, but demonstrates that Chamber II, like Chamber I, can be used in any SEM.

Both microscopes have identical detectors configuration. A SE detector is located on the upper-side of the chamber. A semiconductor BSE detector is located at the bottom of the microscope column. The distance between the membrane and the BSE detector was chosen between 8 and 20 mm. The SE detector includes a grid at positive potential to collect with high efficiency of the SE. The SE detector is also sensitive to BSEs. However, we measured that the collection of BSEs remains low (see below). The semiconductor BSE detector is sensitive to electrons above a certain threshold energy, usually around 7 to 8 keV, and is thus insensitive to SE electrons and low energy BSE.

The membrane is the main element in this method and must have several important properties. First, it needs to be as transparent to electrons as possible. This implicates a low average atomic number (low Z) and a low density. Polymer films are therefore the most adequate choice. The membrane must also resist high pressure differences, be flexible enough to handle in preparation of the sample and should have no porosity to ensure proper sealing of the chamber.

A priori, it was expected that the electrical conductivity of the membrane should be high enough to prevent the local charging of the external surface of the membrane, which may blur the image. A thin conductive carbon film can be evaporated for this purpose on the external side of the membrane. However, we found that at high beam energy, this carbon layer is not necessary and that the liquid medium is sufficient to prevent charging effects. Still, at low energy a conductive layer has interesting features; it not only helps prevent charging effects, but also facilitates imaging through secondary electrons (SE) detection.

Finally, since the sample being observed has to be in very close contact with the membrane, the affinity of the membrane to biological samples may be an important factor. We have tested Formvar, Butvar, and conducting polymers, commonly used in TEM to build supporting films,[15,16] and polyimide, to build the membrane. Only the latter fulfills all the properties required. We used commercially available polyimide membranes of nominal value (given by the supplier) of (1450±140) Å thickness. We verified the thickness with an atomic force microscope, and got a value of (1480 ±120) Å for the sample we tested. A grid was attached to the external side of the membrane (TEM Ni 125–330 μm mesh were used) to reinforce it against the difference of pressure. A carbon deposition of 50 Å on the external surface was sometimes performed. Affinity properties were adjusted by chemical surface treatment of the membrane. For example, biological cells were grown on the membranes treated first with the extracellular matrix proteins fibronectin or laminin. Formvar membranes coated with carbon (total thickness between 50 and 70 nm) have been used with the ''low pressure'' Chamber II and are described in Sec. VI.

III. MECHANISM OF CONTRAST FORMATION

There are two different contributions to the formation of a signal on the detector (see Fig. 2). The first is a source of uniform noise, while the second includes the signal:

(1) When the beam hits the membrane, backscattered electrons (BSE) and secondary electrons (SE) are produced by the membrane itself. Only the SE produced in the first few nanometers (the mean free path of secondaries), can escape from the membrane.[17] This contribution is homogeneous since both the composition and the thickness of the membranes we use are the same everywhere. In the following, the suffix m (*membrane*) will refer to this contribution.

(2) The portion of electrons from the beam which is not backscattered when crossing the membrane impinges upon the sample. Again, secondary electrons and backscattered electrons are produced. The SEs produced here have no chance to escape. In contrast, BSE created in the sample have the possibility to exit back out through the membrane. As they cross the membrane, they may generate secondary electrons which, if created at a distance from the surface which is below their mean free path, can escape to the detector. This second contribution to the signal is the result of the backscattering events in the zone of interest, which reach both the SE and BSE detectors. In the following, the suffix s (*sample*) will refer to this contribution.

The second contribution (s) is obviously the contribution of interest. It carries the information we seek while the first is related to the membrane only (m). A contrast between two neighboring points will be observable if the difference in the sample signal between them is higher than the fluctuations in the whole signal.

Given two different materials for which the backscattering coefficients are known and for a specific membrane, we would like to determine the conditions needed to form an image.

The total signal collected S is composed of both secondary electrons and backscattered electrons:

$$S \sim \epsilon_{\mathrm{BS}} \eta + \epsilon_{\mathrm{SE}} \delta, \tag{1}$$

η and δ represent, respectively, the ratios of BSE and SE currents to the beam current. The coefficient ϵ represents the collection efficiency for the two kinds of electrons that are detected. The backscattering coefficient η is on its own made of two contributions: BSE from inside the membrane (m) and BSE from inside the sample (s):

$$\eta = \eta_m + \eta_s .$$

Similarly, the SE scattering coefficient δ has two contributions:

$$\delta = \delta_m + \eta_s \Delta_m .$$

While δ_m represents the secondary electrons generated by electrons of the beam entering the membrane, Δ_m represents the secondaries generated in the membrane by electrons on their way out, after a relevant backscattering event inside the sample. The backscattering coefficient η_s thus multiplies Δ_m, because the flux of energetic beam electrons traveling back through the membrane is reduced from unity by η_s.

The SE emission coefficient Δ_m may contain a slow material dependence. Depending on the material located below the membrane, the energy spectra of the BSE can vary, and different energies of BSE may in turn have different efficiency to generate SE emissions.

Note that the definitions of backscattering and secondary coefficients we use and the coefficients usually described in the literature differ slightly. The latter are defined for a semi-infinite medium and are characteristic of the material (gold, carbon, nylon, etc.). Here, the coefficients describe the charge emission for a membrane with its particular thickness and its carbon shield. They do not describe the charge emission of a semi-infinite sample of polyimide material. In the same way, the sample coefficients describe the signal coming from the material inside the sample but covered by the membrane. One of our objectives in the following will be to compare experimentally the measured coefficient to the classical theoretical coefficients characteristic of the material itself (e.g., water, gold, etc.).

Let us consider two adjacent points that give signals S_A and S_B. The material contrast between them is defined as

$$C_{AB}=(S_A-S_B)/S_A \tag{2}$$

(assuming $S_A>S_B$). There are two basic ways to modify the signal S. One is to multiply it by a constant (amplification). The other is to add a positive or negative constant to the signal (this is the ''black level''). The contribution of the membrane to the signal is the same everywhere. Its thickness and its composition are very well defined so that neither composition contrast nor topographic contrast appear between points A and B because of the membrane. Contribution m is thus a constant that can be removed by an appropriate choice of the black level. Note that noise on the order of $\sqrt{n}$ where n is the number of electrons scattered from the membrane, may interfere with the measurement, but we ignore it here, returning to it in the next section. With this choice, the contrast between points A and B is greatly simplified:

$$C_{AB}=(\eta_{S_A}-\eta_{S_B})/\eta_{S_A}. \tag{3}$$

The material contrast is related to the difference in the number of backscattering events occurring in the materials located below the membrane on points A and B.

IV. PASSAGE OF ELECTRONS THROUGH THE MEMBRANE

We proceed now to study experimentally the membrane characteristics and quantify that portion of the signal which is related to the membrane only and was suppressed in the expression of the contrast [Eq. (3)] by an appropriate choice of the black level. We do this in terms of BSE and SE emitted from its surface as a function of the energy.

For this purpose we used four different samples and an assembly that allows the different samples to be inserted simultaneously inside the microscope (in practice, only three could be inserted together in the SEM chamber, so we repeated the experiment with overlapping trios and identical conditions). For different energies, the beam was positioned successively on each sample and the current between the ground and the sample was measured.

Sample A is just a Faraday cup,[18] used to measure the beam current I_b by collecting all the beam. Sample B is identical in design except that the aperture is covered with a membrane. We call this measurement I_m. Sample C consists of a pure gold sample connected to ground and covered by a membrane. The gold was first melted so that its surface was smooth enough to obtain large areas where a direct contact with the membrane was achieved. Finally, sample D is our experimental chamber, containing water and sealed by a membrane. Samples C and D define two values for I_s, where s refers to gold or water.

The difference of currents measured on samples A and B, normalized by that of sample A, gives the percentage of electrons emitted by interaction with the membrane. This measures the sum of the secondary and backscattering coefficients of the membrane:

$$1-I_m/I_b=\eta_m+\delta_m.$$

Similarly, the percentage of electrons emitted by interaction with the membrane plus the material located below is the difference of A and C or D:

$$1-I_s/I_b=(\eta_m+\delta_m)+\eta_s(1+\Delta_m).$$

The three measurements are shown in Fig. 3(A). For energies below 5 keV, the gold and water curves are seen to superpose on the membrane curve. This means that the beam is not energetic enough to reach the sample and send BSE back to the detector. Above 5 keV, the three curves differ; a growing portion of the signal detected is provided by the interaction with the material below the membrane. For the water sample and incident electron energy of 10 keV, beam–membrane interactions contribute 50% of the charge emission. Their contribution decreases to 35% at 15 keV. In the case of gold, because of its high atomic number, the membrane contribution falls to 2% at 15 keV.

The next step is to subtract the membrane component and obtain the material contribution to the signal [Fig. 3(B)]. This includes only electrons that are scattered by their interaction with the material of interest (η_s), and potentially also secondary electrons they generate when reaching the surface of the membrane ($\eta_s\Delta_m$), which are sometimes referred to in the literature as secondary electrons of the second kind SE_{II}.[17] At low energies the electrons of the beam do not reach the samples and the curves should be zero. At very high energy, the curves should follow the behavior of the backscattering coefficients of the materials, since the membrane becomes practically transparent. This is what we observe on the two curves. The decreasing slope of the water curve follows the theoretical behavior of the backscattering coefficient, as calculated from Hunger and Kuchler's derivation[19] (see also Ref. 17.) The increasing slope of the gold curve also follows directly the calculated backscattering coefficient evolution with energy (as derived from the same expression).

Normalizing these curves by the backscattering coefficient of the respective materials (with their appropriate energy dependence), we get curves where only a low material dependence remains [Fig. 3(C)]. The transparency of the membrane as defined here is dimensionless, being the ratio of the expected number of backscattered electrons to the total number of charges that actually carry sample information (BSE plus the SE they generate on their way out). This

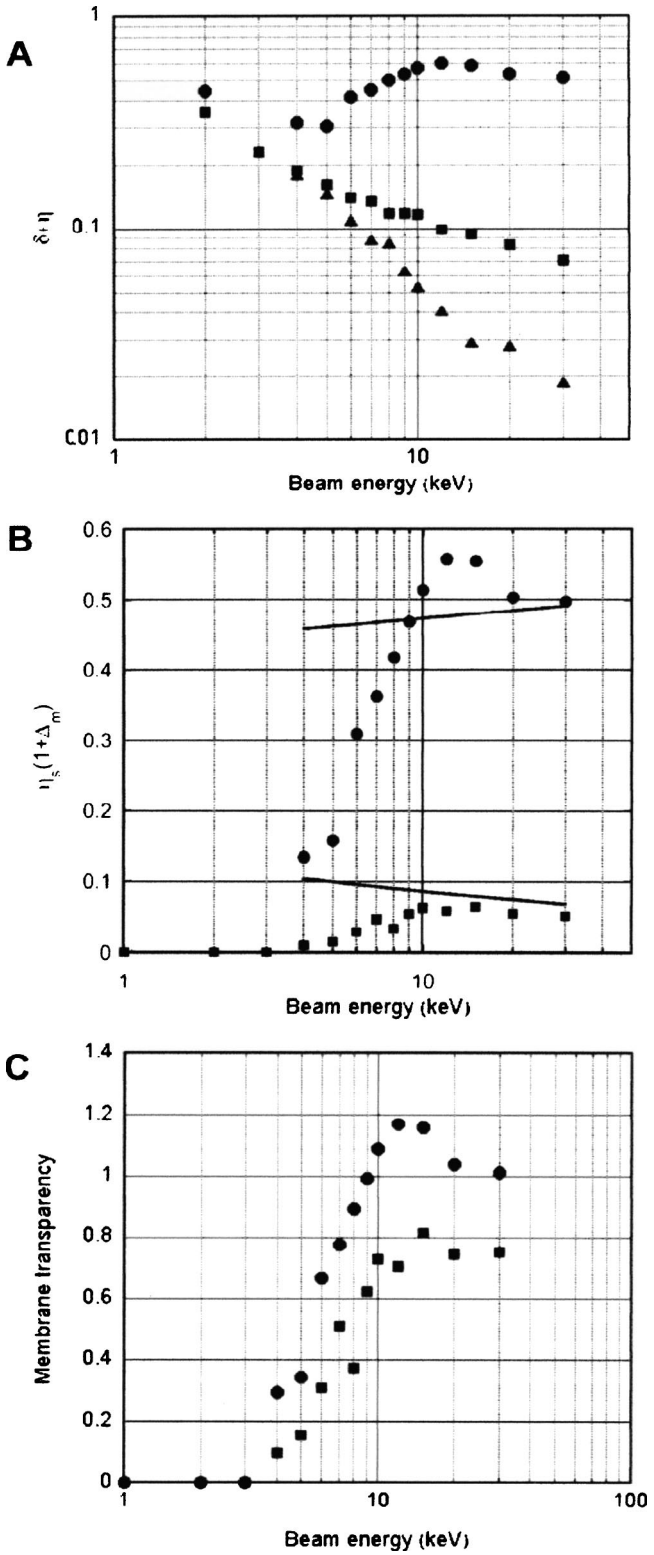

FIG. 3. (A) Sum of the secondary and backscattering coefficients: Triangles represent the membrane signal: $\eta_m+\delta_m$. The circles (gold) and the squares (water) represent the total emission from the membrane and the sample together: $(\eta_m+\delta_m)+\eta_s(1+\Delta_m)$. (B) Sample signal: $\eta_s(1+\Delta_m)$: The lines represent the backscattering coefficients as deduced from Hunger and Kuchler expression. (C) Sample signal divided by the corresponding theoretically determined backscattering coefficient.

choice of normalization makes it especially intuitive as to why deviations below and especially above unity may be interesting.

We attribute the observed small difference between the water and gold curves to different effects. One of them could be a slight overestimation of the backscattering coefficient of water with the Hunger and Kuchler expression. To our knowledge, experimental data on the backscattering coefficient of liquid water could not previously be obtained with other techniques. Our method can be used for such a measurement at high energies, when the membrane effect is negligible. The second reason could be a filtering property of the membrane, since it is known that the energy spectra of BSE emitted depends on the material considered.[17,20] The energies range from 0 to E_0, where E_0 is the energy of the incident electrons. A light material (e.g., carbon) has a distribution that is approximately centered on the value $E_0/2$ and is symmetric. A heavy material (e.g., gold) has a distribution of BSE that is strongly asymmetric, with a peak closer to E_0. This difference has several consequences. First, the ratio of BSE that are able to cross back through the membrane to the total BSE produced is higher for heavy materials than for light ones. Thus, the membrane enhances artificially the contrast between light and heavy elements. Second, the difference in energy spectra of BSE can also influence the SE emission Δ_m since low energy BSE have a higher probability to generate SE on their way out. At 30 keV, we observe a discrepancy of 25%, which we believe results from both membrane related effects and an overestimation of the backscattering coefficient.

The secondary emission Δ_m, is high at intermediate energies. The peak on the gold curve which reaches a value higher than 1, demonstrates this. We suspect it decreases at high energies, because energetic BSE generates less SE on their way out.

The two curves of Fig. 3(C) represent two extreme possible cases of low and high atomic numbers. For other materials of atomic number between that of water and gold, the corresponding curve will lie between the two extremes shown.

We summarize our conclusions from the results up to now as follows. For energies below 4–5 keV, no signal from the sample can be detected. This threshold can be decreased by using thinner membranes. In the intermediate region of energy, Δ_m (the coefficient of SE creation in the membrane by BSE on their way out after interacting with the sample) is high. The membrane converts the BSE signal to a SE signal and it is possible to image with the SE detector. This is illustrated by Fig. 4(A) which shows milk imaged with SE. To verify that this image is not formed by BSE hitting the SE detector, we have placed a negative tension to the grid located at the entrance of the SE detector. This results in canceling the collection of SE, while keeping the collection of BSE approximately unchanged. The signal at the detector was significantly decreased, resulting in a noisy image with almost no contrast. This allows us to conclude that images formed with the SE detector are made mainly from a SE signal. It is unusual in SEM to image only with SE resulting from the interaction of the BSE getting out the sample. This is a particularity of our method in which the SE signal resulting from the incoming beam can be completely removed by adjusting the black level since it is the same at any point scanned. In the same intermediate region of energies, the

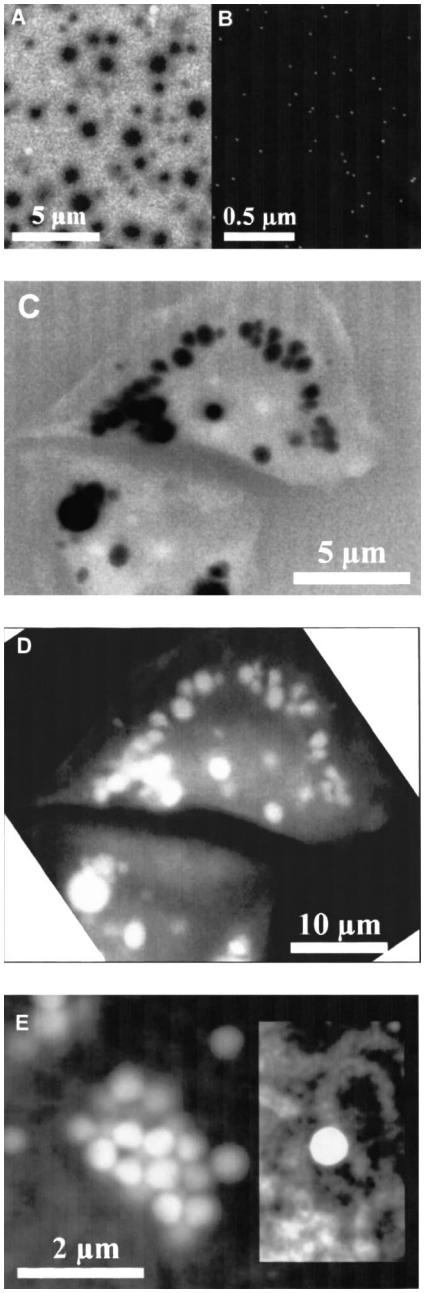

FIG. 4. (A) Milk: fat droplets appear dark on the background of the water which appears bright. As described, this image was collected by the SE detector, and originates in BSE crossing the membrane and creating SE as they traverse it. (B) Gold beads (diameter 20 nm) in water, attached to the membrane. (C) Unstained Chinese hamster ovary cells grown on a fibronectin coated membrane, fixed. (D) The exact same cell as (C) after 5 min treatment with OsO4. (E) Two different contrast enhancements show different aspects of lipid droplets inside a single CHO cell stained with OsO4. The organized packing of lipid droplets is shown in low contrast (most of image), while a rectangle in the image has been strongly enhanced, and shows structures inside the cell. These are most probably mitochondria, which may be expected to be found in proximity to the droplets. Such an enhancement saturates the droplets' image. Images were acquired with the Philips microscope at 30 keV with the BSE detector, except (A) obtained in the JEOL microscope with the SE detector at 12 keV.

membrane cuts a part of the BSE emitted by light materials, enhancing the contrast between heavy and light materials. For high energies, the charges emitted approach the theoretically predicted BSE coefficients (Δ_m diminishes and η_s approaches η) and it is easier to image using the BSE detector [Figs. 4(B)–4(E)].

TABLE I. Evaluation of the minimum current needed for different samples containing water. I is calculated from the Eq. (4). η are calculated with Hunger and Kuchler expression at $E=20$ keV, using the mean atomic number Z indicated. A scanning time of $T=100$ s is assumed.

Material	Z	η	Contrast to water	I (pA)
Water	7.22	0.075		
Cells	7.07	0.073	0.027	2900
Oil	5.8	0.055	0.267	30
Gold	79	0.78	0.90	0.25

V. DEDUCING A MINIMUM PROBE CURRENT

As soon as a small difference in the mean atomic number exists between two points, it is theoretically possible to observe it. The question is how many electrons are needed to make an observation. Such an estimate is useful since it indicates the ease and the feasibility of an observation. When high doses are required, charging and radiation damage are more of a problem. Also, high currents cause a lower resolution because the beam is less focused, and too long integration times may be damaging and are inconvenient.

We calculated the minimum current required to image specimens of specific contrast using the *threshold equation*,[21] described in detail in Goldstein *et al.*[17] Adapted to our case this equation is written as

$$I_B > 16/\eta_s T C^2 \quad \text{(pA)}, \tag{4}$$

where η is the backscattering coefficient of the specimen and T the image scan time in seconds.

Results concerning biological specimens such as a cell, an oil/water emulsion and a gold particle in water are shown in Table I. A scan time of 100 s was assumed. The results are strictly valid for high energies, for which the contrast C is simply related by Eq. (3) to the backscattering coefficients of the materials below the membranes. A cell surrounded by an aqueous medium presents a low contrast, and furthermore the backscattering coefficients are low.[24] The minimal current required is then in the range of nano-Amperes (nA). An oil/water emulsion presents a contrast ten times higher. The minimal current falls in that case to a few tens of pico-Amperes (pA). Finally, a high contrast sample like gold particles requires only a fraction of a pA.

These results match our experimental observations. Emulsions of oil/water, like milk, can be observed directly in standard conditions of current and integration time [Fig. 4(A)]. These images can be compared with those obtained on images of emulsions using the ESEM.[22] The resolution using the wet SEM is better by a factor of about five. We have further compared the two techniques and find that the absence of continuous evaporation and condensation in the wet SEM and the ability to work at room temperature are a distinct advantage.

A biological sample such as a cell needs a high current to be imaged in a reasonable integration time [Fig. 4(C)]. Even under these conditions, the observable details are often

close to the detection limit. One can advantageously use labeling with heavy markers such as colloidal gold particles [Fig. 4(B)] to decorate the cell or stains like uranyl acetate or OsO4. Figure 4(D) shows the same cell as in Fig. 4(C) after treatment with OsO4. The OsO4 scatters very strongly, and creates a strong contrast. The contrast difference of Fig. 4(D) with the unstained cell in Fig. 4(C) is not quite evident due to the digital image processing that strongly enhances the contrast in Fig. 4(C). Figure 4(E) shows an assembly of lipid droplets in a cell treated with the same stain. The signal created by the heavy metal markers is so strong that it obliterates other details in the cell. We therefore enhanced a rectangular region at the right side of the image, bringing our details in the background. The lipid droplet is seen to lodge in the midst of a number of elongated organelles, which we have identified using uranyl acetate staining as mitochondria.[14]

VI. RESOLVING SMALL DETAILS AT DIFFERENT DEPTHS

Perhaps our strongest and most surprising result, and one we need to understand, is that the experimental resolution is orders of magnitude better than what could be predicted theoretically. It turns out that the resolution obtained with the wet SEM depends on the size and distance from the membrane, and not only the composition of the object observed. We first show that the naive estimate based on the volume of interaction does not fit the actual measured resolution. The understanding of the measured resolution then rests on the role of inclusions that are near the membrane. As we explain below, the mechanism for resolving small inclusions relies on the existence of a small, high resolution signal riding on a large, sometimes noisy, background. The resolution is ultimately limited by the size of the electron beam and determined by the issue of contrast and the associated detection capability.

The naive theoretical calculation of the resolution is based on the effective signal producing volume, characterized by the Kanaya–Okayama range R_{KO}. This is the typical radius of the volume of interaction of the electrons inside the material:

$$R_{\mathrm{KO}}=0.0276(A/Z)Z^{0.11}E_0^{1.67}/\rho,$$

where R_{KO} is expressed in μm, E_0 is the incident beam energy in keV, A is the atomic weight in g/mole, ρ is the density in g/cm^3, and Z is the atomic number. In the case of a gold sample, 80% of the BSE originate in a volume of diameter $d_{\mathrm{BSE}}=0.4R_{\mathrm{KO}}$, for carbon it is $d_{\mathrm{BSE}}=1.0R_{\mathrm{KO}}$.[17] Here the distance d_{BSE} is the mean diameter of the volume covered by electrons in the sample before returning as BSE.

If the sample is mainly water, a simple approximation is that the membrane and the sample have close enough atomic numbers to be estimated as identical. Then, the resolution is simply

$$d_{\mathrm{eff}}=(d_B^2+d_{\mathrm{BSE}}^2)^{1/2},$$

where d_B is the diameter of the beam entering the membrane, which depends on the microscope electron source.[23] Considering an average density $\rho=1$ and a beam size in the nanometer range,[23] this theoretical estimation then predicts a resolution of a few microns at 10 keV, while at 20 keV, it goes up to 10 μm!

Luckily, the resolutions obtained experimentally are few orders of magnitude better. This is because the volume scattered by the BSE depends strongly on its entry point. Variations in the composition close to that entry point (i.e., adjacent to the membrane) affect both contrast and resolution by strongly influencing the subsequent scattering of the electrons. Small inclusions can be imaged with a much higher resolution and include, for example, gold particles that label specific proteins in a cell, cell organelles stained with heavy materials, or fat droplets in milk.

A. High contrast inclusions

For gold particles inside water, the scale of the volume of interaction is about a micrometer, while the scale of a the resolution obtained experimentally at high energy is about 10 nm [see Fig. 4(B)]. Beads of actual diameter 40 nm appear to be around 45 nm diameter at 30 keV. Beads of 20 nm diameter appear to be around 23 nm. The resolution is actually related to the diameter of the beam when reaching the depth at which the particle is located, not to the volume of interaction of BSE.

The important point is the following. At high energies, the beam can diffuse inside the water if there is no bead to intercept it, and the volume sampled by the BSE is deep and wide (up to 10 μm as seen above). The signal that the BSE generates is the result of integrating over a very large volume and for this reason, does not vary significantly when the beam is scanned. Furthermore, at high magnification, when the image size itself is on the order of the size of the BSE sampled volume, this deep BSE signal is a constant that can be removed by an appropriate choice of the black level. On the other hand, when the electron beam crosses a heavy material bead, a significant part of the beam is intercepted and immediately many more BSEs are emitted because of the high backscattering coefficient. Thus, the resolution obtained is dependent on the spatial extension of the electron beam when reaching the particle.

A bead that is located just below the membrane is imaged with the best resolution because the spreading of the beam is the lowest at that point. The deeper the particle inside the sample, the lower is the resolution at which it can be imaged.

The spreading of the beam is a problem that is well adapted to solution by Monte Carlo simulations. We used a code devised by Joy[25,26] to perform such a calculation. Input values for the simulation are the polyimide stoichiometric formula $C_{22}O_5H_{10}N_2$, the mean atomic number 6.4 and the mean atomic weight 9.8 g/mol. The density of the material is 1.4 g/cc.

Figure 5(A) shows the evolution of the 68% beam broadening diameter with energy, as determined from simulations using an incident beam of zero diameter and normal incidence. At 20 keV, the limit of resolution just below the 1450 Å thick membrane is estimated at 18 nm. At 30 keV, the beam diameter at the same position would be 10 nm. The

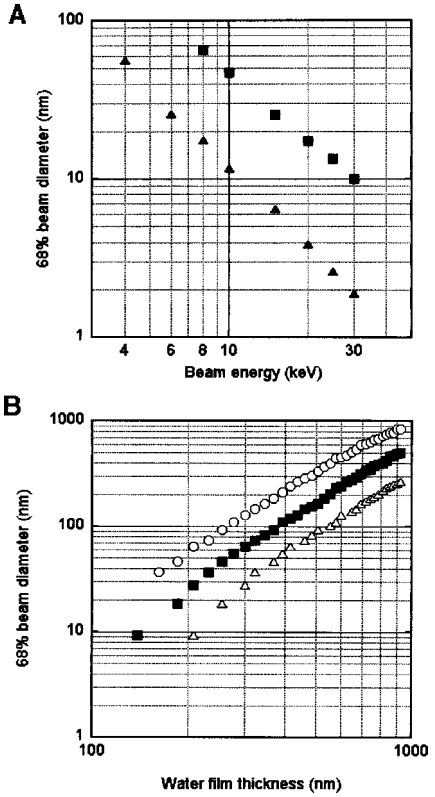

FIG. 5. (A) Monte Carlo results for the beam diameter d_m after crossing the polyimide membrane. The squares are for a foil thickness of 1450 Å, the triangles for a membrane which is half as thick (700 Å). The values correspond to the 68% beam broadening diameter with an incident beam radius of zero. Taking into account the lateral extension of the incident beam, the effective beam diameter after crossing the membrane is given by $d_{\text{eff}} = \sqrt{d_b^2 + d_m^2}$; (B) Monte Carlo simulation results for the 68 broadening diameter d_{water} after crossing a water layer, at 15 keV (circles), 20 keV (squares), and 30 keV (triangles). Those values were calculated assuming that the beam radius is zero entering into water. The effective beam diameter is given in total by $d_{\text{eff}} = \sqrt{d_b^2 + d_m^2 + d_{\text{water}}^2}$.

choice of 68% beam width is somewhat arbitrary, and is dependent on the efficiency of the particular detection system in use. It was made according to the experimental results with the 20 nm gold beads in contact with the membrane. A 90% portion would yield a resolution two times lower than what is observed. The simulation predicts that using a membrane of identical density and mean atomic number but twice thinner enables imaging with 10 nm resolution. We verified this experimentally with the ''low vacuum'' Chamber II and carbon coated Formvar membranes of 50–70 nm thickness (the manufacturer does not give definite thickness for these membranes, and they may vary between these two extremes); 10 nm gold particles stuck to the membrane could be resolved, appearing as object of ~15 nm at 20 keV (data not shown).

To calculate the resolution for inclusions located deeper inside the sample, one must also take into account the spreading of the beam which results from crossing the layer of water in between. An approximation is given by $d_{\text{eff}} = (d_b^2 + d_m^2 + d_{\text{water}}^2)^{1/2}$. The beam scattering d_{water} calculated from Monte Carlo simulations is shown in Fig. 5(B). Summing the different contributions estimated, at 30 keV, a particle located at 200 nm below the 1450 Å membrane should be imaged with a resolution around 14 nm ($d_b = 1$ nm, $d_m = 10$ nm, $d_{\text{water}} = 10$ nm). At 500 nm depth, the resolution is around 100 nm and at 1000 nm depth, it is a few hundreds of nanometers.

Resolution is not the unique factor which determines whether inclusion imaging is good quality or not. Whether an object can be resolved or not also depends on how well it is detected. A second determinant factor is the contrast these objects produce. We first discuss this for high contrast (large Z) materials, and in the next subsection discuss the issue of low contrast (low Z) materials.

As a first illustration, we note that 20 nm gold beads in contact with the 1450 Å polyimide membrane were imaged with very good resolution while 10 nm were not even detected. This is because when the beam size is by a factor two or three times larger than the object, the signal amplitude is very low. A heavy inclusion is detectable if its size and the beam size are close together. If the object is smaller, the contrast is lost.

Also, when considering a smaller and smaller particle size, the probability to generate BSE decreases. At high energies, the cross section for scattering of electrons decreases, and the BSE sampling depth in gold reaches the hundred nanometers scale. For example, at 30 keV, it is in the range of 150–300 nm ($0.1-0.2R_{\text{KO}}$). When considering a particle smaller than these values, a large proportion of the beam may cross it without interaction. Thus, for the same amount of electrons hitting it, a ten nanometers particle generates less BSE than one of 20 nm. The first conclusion to draw is that, to image small inclusions, we need higher currents then those estimated in Sec. III which are strictly valid for large objects. Furthermore, when increasing the energy to get the best focused beam, we may lose more signal. Our experiments show that the particle size at which this becomes a real problem is very small in the case of gold and is ~10 nm.

For completeness, it is of interest to evaluate how deep an inclusion can be detected inside the sample. Considering that a heavy particle can be detected if its size is comparable to the beam size, the values of beam spreading calculated above should indicate the particles that can be observed at the considered depth. With the membrane used and at 30 keV, a 20 nm gold particle is visible until 250 nm below the membrane, a 40 nm diameter one should be detectable until ~340 nm, and 100 nm until 550 nm. These values differ for other energies, raising the intriguing possibility of obtaining depth information by varying the beam energy.

B. Low contrast inclusions

The case of light material inclusions presents many similarities with the previous situation. With milk, we were able to image details down to 100 nm. We were surprised to get better results with emulsions than with beads of similar material composition, and attribute this to the fact that emulsion droplets may wet the membrane. They can deform exposing more material in contact with the membrane. Here, again, the resolution obtained is far better than the size of the volume sampled by the BSE.

The best resolution for light inclusions should be similar

to those of gold particles and be related to the diameter of the beam. In practice, this is not so, and our ability to detect small light inclusions in water is limited more by contrast than by beam size. This is illustrated by the fact that while latex beads smaller than 150 nm are hard to observe in pure water even with high probe current and long integration times, 93 nm latex beads immersed in a solution containing a heavy elements like Na I salt at high concentration (4 M), were easily resolved.

The limit on the smallest light inclusion size detectable is thus related to the ability to distinguish between small variations in BSE emission. While for gold beads, this limit seemed to be below 10 nm, for carbonaceous compounds in water the limit is approximately ten times higher.

VII. RADIATION DAMAGE

One well-known limitation on the ability to image biological and organic samples is the structural damage caused by the radiation of the beam. A typical value for damage of biological material by radiation is 0.1–1 electrons per $Å^2$. The limit for nonbiological materials may be higher, although we have seen that much beyond these values (up to ten times the dosage) actual damage can occur in the sample. Examples for such damage are the production of bubbles in fluids, movement and rearrangement of objects in the image, and detachment of parts of the sample from each other and from the membrane.

For example, the milk depicted in Fig. 4(A) was imaged repeatedly and showed no signs of damage. In general, emulsions such as this one consistently give a better contrast than similarly sized polystyrene beads, which have very similar carbon content. We can therefore deduce that the oily droplet wets the polyimide membrane, bringing more carbon atoms into close proximity of the membrane. The droplets can still move around, and some slight rearrangement is observed over consequent images. Total disruption of the emulsion can be attained at very high beam currents, typically ten times our normal operational limit. Violent motion of the fluid can then be observed.

For biological samples the problem is more complex, and has been the subject of intense investigation in the literature. At these radiation levels not only DNA but also proteins are being harmed. We have seen that changes in living cells, once they were scanned, occur progressively. After beam exposure, cells were observed by phase contrast microscopy. The first visible sign of change in large organelles occurs after about 20 min. On a longer time scale, we could observe some cells losing their nucleus or getting detached from the substrate. This indicates that, although the cell is damaged and may be dead or dying, structural changes occur on a much slower time scale than the scanning time. This time scale is most probably determined by biological processes of damage and decay.

Far below the threshold of visible structural damages, irradiation can lead to cell death after a short or a long period of time. Wet SEM in fact enables the performance of cell survival assays as a function of radiation dose. We have conducted such a preliminary study using Trypan Blue dye as an indicator of cell viability. While this is a gross indicator, after receiving the radiation typical of a high resolution scan, all cells we observed showed an uptake of dye, indicative of cell death. Only at about a thousandth of this did a considerable percentage of the cells resist the uptake of the dye. These results indicate that high resolution imaging of cells that continue to live even a short period like 15 min, is not possible at present. Hardier cells such as the bacterium *Deinococcus radiodurans* may give different results, and the addition of scavenger molecules to reduce the amount of free radicals created by the beam may also provide a way to alleviate the damage.

There are two different questions related to levels of damage. First, is there only little or no noticeable structural damage, so that what we observe is in reality how the cell is organized? The second is the issue of lethal damage to the cell, i.e., are we killing the cell and can we make any dynamical experiment. To the first question, our results indicate that structural damage occurs on a time scale much longer than the image acquisition. To the second question, we believe we cannot make a reliable dynamical experiment because the cells are dying after the first exposure.

VIII. DISCUSSION

Using our new technique, the full power of the SEM can be brought to bear upon the imaging of liquid samples, including wet cells, emulsions, and any other material of interest. That full power is in practice limited by the physics of electron–matter interactions, and these constraints must be kept in mind when designing optimal experiments with the Wet SEM. The membranous partition has little or no influence on the resolution and contrast of BSE in comparison to a regular SEM. Still, the strongest physical constraint is probably that the resolution of SEM in soft (low Z) material turns out to be about 100 nm, only slightly better than the optical resolution. This resolution is still orders of magnitude better than what might have been expected using naive theoretical considerations. For high Z materials the resolution is on the order of 10 nm, more in line with the standard (but also high Z!) SEM usage. Imaging 20 nm particles is easily achieved when these are located in proximity of the polyimide membrane, as well as 10 nm particles with a twice thinner membrane. Imaging of deeper inclusions requires them to be larger: a 40 nm gold particle is visible and resolved until $\sim$350 nm. This also allows some three-dimensional information to be gleaned.

To our knowledge no other technique allows this kind of measurement. The closest in comparison is probably soft x-ray microscopy, whose limitation is that it requires very heavy equipment.[27] Only the wet SEM technique would allow simple, fast, and routine experiments at these resolutions.

Wet SEM has many interesting features for cell biology. Some cell organelles produce enough contrast to be visualized directly. In most cell lines, these are generally the nucleus, nucleoli, the cell membrane, and the lipid droplets. This constitutes an original way of imaging in the context of

cell biology since contrast originates from the materials mean atomic number.

Beyond the highly visible organelles, the difficulty to image biological samples without any staining is real. However, many biological issues can be visualized by the use of high atomic number stains and labels. Staining and specific labeling are, as a matter of fact, techniques commonly used for both electron and optical microscopies in biology.

The development of nondestructive stains for biological cells is an important direction for further improvements. We used with success ferritin, a protein rich in iron atoms, to image cells. The development of recombinant ferritin as a marker for SEM is an obvious next step, taking care to avoid an iron imbalance in the cell.

On the technical side, several improvements can be seen. The development of stiff, thinner membranes could allow working with a larger range of energies. The secondary emission results for the main part from the carbon layer deposited on the membrane. Enhancing this emission using other material could be of interest for the detection at low energies. Effectively, using the backscattered electron detector is possible above a detection threshold usually around 7 keV (for a semiconductor detector).

Finally, we believe this technique can also find applications in numerous areas of physics, such as materials research and complex fluids.

ACKNOWLEDGMENTS

The authors thank N. Levit-Binnun, Y. Karni, I. Shariv, and D. Zajfman for insight and advice, J. Fineberg for a critical reading of the manuscript, and E. Klein for help in use of the SEM and O. Yeger for help in staining the cells.

[1] G. Binnig, C. F. Quate, and C. Gerber, Phys. Rev. Lett. **56**, 930 (1986); B. Drake *et al.*, Science **243**, 1586 (1989).
[2] G. Binnig, H. Rohrer, Ch. Gerber, and E. Weibel, Phys. Rev. Lett. **50**, 120 (1983).
[3] U. Durig, D. W. Pohl, and F. Rohner, J. Appl. Phys. **59**, 3318 (1986).
[4] E. H. K. Stelzer, J. Microsc. **189**, 15 (1997); J. T. Frohn, H. F. Knapp, and A. Stemmer, PNAS **97**, 7232 (1999).
[5] W. Denk, J. H. Strickler, and W. W. Webb, Science **248**, 73 (1990).
[6] G. D. Danilatos, Microsc. Res. Tech. **25**, 354 (1993); E. R. Prack, *ibid.* **25**, 487 (1993); G. D. Danilatos, Adv. Electron. Electron Phys. **71**, 109 (1988).
[7] R. F. M. Thornley, Ph.D. thesis, University of Cambridge, 1960.
[8] I. M. Abrams and J. W. McBrain, J. Appl. Phys. **15**, 607 (1944).
[9] E. F. Fullam, Rev. Sci. Instrum. **43**, 245 (1972).
[10] J. A. Swift and A. C. Brown, J. Phys. E **3**, 924 (1970).
[11] S. Murakami, A. Fukami, K. Fukushima, and A. C. Brown, J. Electron Microsc. **26**, 259 (1977).
[12] D. F. Parsons, Ann. N.Y. Acad. Sci. **483**, 157 (1986).
[13] Fujiyoshi *et al.*, United States Patent No. 5,406,087 (1995).
[14] S. Thiberge, A. Nechushtan, D. Sprinzak, O. Gileadi, V. Behar, O. Zik, Y. Chowers, S. Michaeli, J. Schlessinger, and E. Moses, Proc. Natl. Acad. Sci. U.S.A. **101**, 3346 (2004).
[15] E. Davison and W. Colquhoun, J. Electron Microsc. Tech. **2**, 35 (1985).
[16] D. Handley and B. Olsen, Ultramicroscopy **4**, 479 (1979).
[17] J. I. Goldstein *et al.*, *Scanning Electron Microscopy and X-Ray Microanalysis* (Plenum, New York, 1992), pp. 95–113.
[18] Faraday cup is constructed of a bulk of carbon connected to ground, with a cavity (2 mm diameter and 3 mm deep) at its top, closed by a Ni plate with an aperture of 10 μm diameter in the middle. The beam enters through the aperture, hits the bottom of the carbon cavity, so that the main beam and practically all scattered electrons are collected.
[19] H. J. Hunger and L. Kuchler, Phys. Status Solidi A **56**, K45 (1979).
[20] H. Bishop, in *Proceedings of the Fourth International Conference on X-Ray Optics and Microanalysis, Paris, 1966*, edited by R. Castaing, P. Deschanps, and J. Philibert (Hermann, Paris), pp. 153–158.
[21] C. W. Oatley, *The Scanning Electron Microscope* (Cambridge University Press, Cambridge, 1972).
[22] R. G. Mathews, D. J. Stokes, B. L.Thiel, and A. M. Macdonald, Inst. Phys. Conf. Ser. **161**, 95 (1999).
[23] Field emission source produces a beam of 1 nm size in the best conditions (low current, high energy) and 10 nm the worst. A tungsten filament source produces a beam between 10 and 100 nm (Ref. 17).
[24] The four elements C, H, N, and O make up nearly 99% of the weight of a biological specimen like a cell. The cell is composed of 70% water and 29% organic compounds. About 50% of the atoms in these compounds are H atoms, 24% are C, 24% are O, and 1% are N atoms [B. Alberts *et al.*, *Molecular Biology of The Cell* (Garland, New York, 1994)]. Given these values, the mean atomic number of a typical organic molecule is 6.72, that of water is 7.22, and for a living cell, it is 7.07. Calculation of the corresponding backscattering coefficient at 20 keV give 0.075 for water, 0.073 for a cell (Ref. 19).
[25] D. C. Joy, computer code Monte Carlo Simulations of Electron Beam—Solid Interactions, available at www.microanalysis.org, 1991.
[26] D. C. Joy, *Monte Carlo Modeling for Electron Microscopy and Microanalysis* (Oxford University Press, New York, 1995).
[27] C. Jacobsen, Trends Cell Biol. **9**, 44 (1999).